INSTITUTE OF PHYSICS PUBLISHING JOURNAL OF PHYSICS B: ATOMIC, MOLECULAR AND OPTICAL PHYSICS

J. Phys. B: At. Mol. Opt. Phys. **34** (2001) 4919–4938 PII: S0953-4075(01)28150-4

Spatial alignment of diatomic molecules in intense laser fields: I. Experimental results

F Rosca-Pruna[1], E Springate[1], H L Offerhaus[1], M Krishnamurthy[2], N Farid[3], C Nicole[1] and M J J Vrakking[1]

[1] FOM-Institute for Atomic and Molecular Physics (AMOLF) Kruislaan 407, 1098 SJ, Amsterdam, The Netherlands
[2] Tata Institute of Fundamental Research, Homi Bhabha Road, Mumbai 400 005, India
[3] Blackett Laboratory, Imperial College of Science, Technology and Medicine, Prince Consort Road, London SW7 2BZ, UK

Received 21 August 2001
Published 26 November 2001
Online at stacks.iop.org/JPhysB/34/4919

Abstract

We present measurements of the laser induced spatial alignment of two diatomic molecules, iodine (I_2) and bromine (Br_2). Dynamic alignment is inferred from the angular distribution of the ionic fragments from multi-electron dissociative ionization (MEDI). The angular distributions were determined for different pulse durations and energies of the short infrared laser pulses that induce the MEDI, and were measured using a velocity map ion imaging detector. The width of the angular distribution of the fragments with respect to the laser polarization axis depends only weakly on the laser pulse energy, and decreases rapidly for longer pulse lengths (a few picoseconds) at constant pulse energy. The interpretation of this result in terms of dynamic alignment is supported by an extended field ionization Coulomb explosion model that includes the rotation of the molecule induced by the laser field.

1. Introduction

In the last decade multi-electron dissociative ionization (MEDI) of molecules in intense laser fields has drawn considerable interest. A lot of attention has been given to the angular distribution of the fragment ions, which is observed to be strongly peaked along the laser polarization axis. This anisotropy has alternatively been explained in terms of the dependence of the ionization rate on the angle between the molecular axis and the laser polarization axis (geometric alignment) [1] and in terms of a laser-induced reorientation of the molecules prior to or during the dissociative ionization (dynamic alignment) [2]. Improved understanding of the role of rotational pumping and the formation of pendular states in laser-induced dynamic alignment [3–7] and the role of electron localization in multi-electron dissociative ionization [8, 9] has led to the realization that the anisotropy is frequently caused by a combination of geometric and dynamic alignment [10–14].

Individual researchers have used different criteria to distinguish the role of geometric and dynamic alignment. Normand *et al* [15] and Dietrich *et al* [16] performed double-pulse experiments on CO and I_2, respectively, showing that fragment ion signals measured parallel to the laser polarization axis can be depleted by a preceding laser pulse with orthogonal polarization. This suggests that both lasers interact with all molecules in the focus and that the anisotropy is a manifestation of laser-induced alignment of the molecules. Posthumus *et al* argued that the absence of fragment ions at 90° with respect to the laser polarization at high enough laser intensities is a signature of the presence of dynamic alignment [10]. Based on this criterion they concluded that in MEDI of H_2 and N_2 with 50 fs Ti:Sa laser pulses at intensities around 10^{14} W cm^{-2} dynamic alignment played a role, whereas in MEDI of I_2 with the same laser it did not and the anisotropy in the angular distribution was almost completely determined by geometric alignment. Ellert and Corkum used differences in the fragmentation patterns observed with linearly and circularly polarized laser pulses to conclude that Cl_2 is dynamically aligned by 80 fs laser pulses around 625 nm, whereas I_2 is not [11]. Schmidt *et al* inferred the occurrence of dynamic alignment in Cl_2 and N_2 from the dependence of the angular distributions on the molecular parent ion state, the laser wavelength, the laser intensity and the laser pulse duration (130 fs or 2 ps). In the case of I_2, they concluded that dynamic alignment was inefficient under the conditions accessed in the experiment [13]. Similarly, the dependence of the observed alignment on the laser intensity was also used by Banerjee *et al* to distinguish dynamic from geometric alignment [17].

In this paper, we present an experimental investigation of geometric and dynamic laser induced alignment of I_2 and Br_2 molecules. We present experiments where we have used velocity map ion imaging [18] of the fragment ions from MEDI, to study changes in the fragment ion angular distributions when the pulse energy and the pulse duration are varied. The main conclusion from our work is that dynamic alignment of heavy-atom molecules like I_2 and Br_2 strongly depends on the laser pulse duration and is only weakly affected by the peak laser intensity in the focus. For pulse durations $\leqslant$100 fs our experimental angular distributions are determined by geometric alignment, whereas for longer pulse durations dynamic alignment becomes dominant. Our results are supported by an extended field-ionization Coulomb-explosion model that includes the laser-induced rotation of the molecule (see the following paper [19]). Our results show that a measurement of the dependence of the angular distributions on the laser pulse duration clearly distinguishes between geometric and dynamic alignment.

The paper is organized as follows. Section 2 describes the experimental set-up and discusses the advantages of using a velocity map imaging detector in studies of molecular alignment. The experimental results are presented in section 3, where the two subsections present a description of the angular distributions and the kinetic energy distributions of the ionic fragments. The model used to simulate the experimental results is only briefly described in section 4, since it is the subject of a companion paper [19]. In this section, a comparison between the theoretical and the experimental results is presented. Our conclusions are summarized in section 5, where we compare our work to other experiments.

2. Experimental set-up

The experiment was performed using a home built Ti:sapphire chirped pulse amplification (CPA) laser system operating at 50 Hz. This system provides pulses with an energy up to 40 mJ/pulse and a minimum pulse duration of 80 fs at an 800 nm central wavelength. In the present experiment, the laser-molecule interaction was studied as a function of the laser pulse duration and pulse energy. The pulse duration was controlled by adjusting the

distance between the compressor gratings. This puts a frequency chirp on the pulse, which in the absence of resonant intermediate states in the ionization processes, is not expected to influence the experiment. In agreement with this expectation, no dependence on the sign of the chirp was observed experimentally. The sign of the chirp introduced in the pulse was nevertheless kept the same for all the measurements reported here. The laser pulse duration was measured using a single-shot autocorrelator, which was calibrated using a commercial scanning autocorrelator (Femtochrome Research). The pulse duration was varied between 80 fs and 6 ps. The pulse energy was controlled using a half-wave plate in combination with a polarizer, and was varied from 0.75 to 3 mJ, in the case of I_2, and from 0.9 to 3.9 mJ in the case of Br_2. The maximum pulse energy used in the experiments was limited by the appearance of space charge effects in the observed images, which is recognized by the appearance of streaks in the ion images. The infrared laser pulses were focused with an $f = 500$ mm plano-convex lens ($f/D < 100$) yielding a maximum peak intensity of about 2×10^{15} W cm^{-2}. The peak intensity was calibrated in each experiment using above-threshold ionization (ATI) photoelectron spectra of Xe [20]. In these photoelectron spectra peaks due to eight-photon excitation to Xe(4f) and nine-photon excitation to Xe(5g) appear in addition to the non-resonant ionization signal at characteristic laser intensities. Thus, by comparing the photoelectron kinetic energy distributions obtained in our experiment to those reported at a range of intensities by Schyja *et al* [20] the absolute intensity could be calibrated with an estimated accuracy of 10–20%. Furthermore, the ATI spectra were used to calibrate the absolute energy scale of the velocity map imaging spectrometer (see section 3).

The laser was focused onto a pulsed molecular beam formed by running neon (Ne) or argon (Ar) through a cell containing solid I_2 or liquid Br_2, and expanding the mixture through a pulsed valve with a 1 mm nozzle [21] placed 5 cm in front of a 1.5 mm diameter skimmer, that separates the source region from the experimental chamber (figure 1). The I_2 sample was used at room temperature, whereas the Br_2 vapour pressure was controlled by placing the cell in a low temperature bath ($-50\,^{\circ}$C) consisting of a mixture of dry ice, water and acetone. The Ar/Ne backing pressure was adjusted to approximately 2 bar. The partial pressure of I_2 and Br_2 in the interaction region was estimated to be about 10^{-6} mbar, whereas the pressure of the Ar/Ne carrier gas in the interaction region was about 10^{-3} mbar. In order to avoid space charge effects, care was taken to ensure that experiments were only conducted where the observed Ar^+/Ne^+ signal was less than one order of magnitude larger than the I^+/Br^+ signal. The absence of space charge effects was confirmed by repeating some of the measurements at reduced sample pressures (obtained by detuning the timing of the pulsed gas valve with respect to the firing of the laser). The gas inlet lines were replaced between the I_2 and the Br_2 experiments, to avoid contamination of the recorded signals due to the presence of IBr. The background pressure in the experimental chamber was 1×10^{-9} mbar.

The laser and the molecular beam entered the vacuum chamber horizontally at 90° with respect to each other, and intersected at a point located between the repeller and extractor of a velocity map ion/photoelectron imaging detector [18], which was mounted perpendicular to the plane defined by the molecular and laser beams (figure 1). The linear polarization of the laser was kept in the horizontal plane (i.e. along the molecular beam). The velocity map imaging detector consists of a repeller plate and two accelerator electrodes, the second of which forms the entrance to a 50 cm long field-free flight tube which was held at ground potential. Depending on the polarity of the voltages applied to the repeller and the extractor, ions or electrons created in the interaction region are accelerated towards the detector. The detector consists of a dual microchannel plate detector (MCP) followed by a phosphor screen. The MCP and the phosphor screen are capacitively coupled and therefore the whole detector

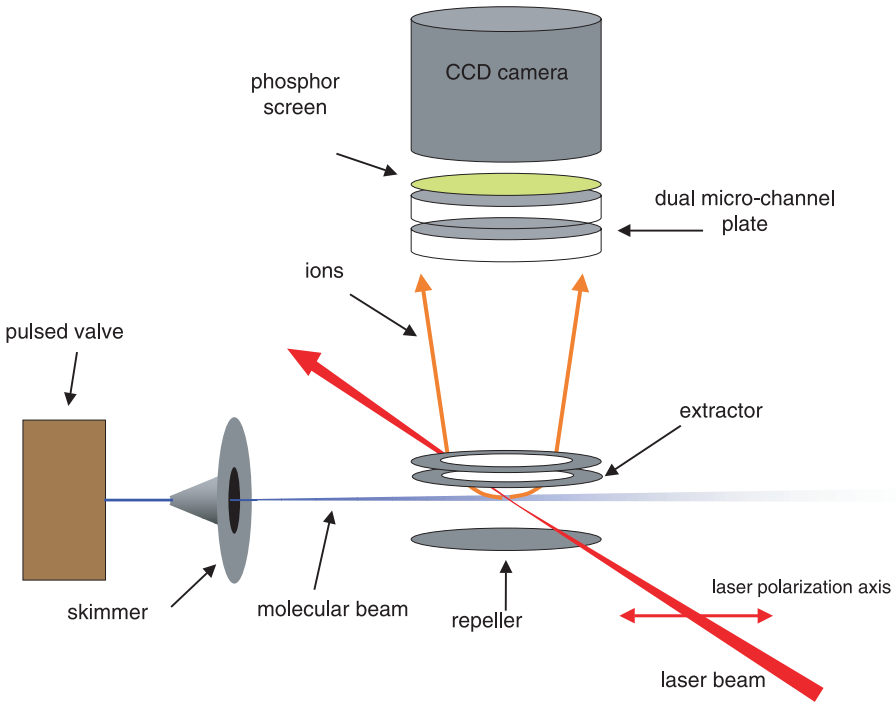

Figure 1. Schematic of the experimental set-up used, showing the molecular and laser beam propagation directions and the ion imaging system.

assembly can be gated in time with a gate width of ∼100 ns, enabling measurements for individual m/q ratios (m is the mass of the fragment and q is the charge of the fragment). The signal on the phosphor screen was recorded by a CCD camera (Pulnix), transferred to a computer at a 30 Hz repetition rate and stored and analysed by a LabVIEW data acquisition program. On this system the data acquisition can be done in two modes: an analogue mode and a counting mode. In analogue mode the signal measured by each pixel of the CCD camera is stored without any further analysis. In counting mode the centre of each spot on the phosphor screen corresponding to an ion/electron is determined and stored [22]. In this mode the signals have to be kept sufficiently low to ensure that there is no overlap between different ions on the phosphor screen. In the present experiment the analogue mode was used, to avoid the latter problem while varying the experimental conditions over a wide dynamic range.

A major advantage of velocity map imaging over the time-of-flight technique which has frequently been applied to studies of intense field dissociative ionization is the fact that the images created on the phosphor screen represent a direct projection of the 3D velocity distribution of a particular fragment ion onto a 2D plane. Therefore, angular distributions can be measured directly without having to perform series of measurements where the laser polarization is rotated with respect to the detector axis. Velocity map imaging has a very high sensitivity, since the ions are projected onto the MCP detector with unit efficiency. Apart from the statistics of the experiment, the angular and kinetic energy resolution are only limited by the number of pixels of the CCD camera and are typically better than one degree and one per cent, respectively. In the present experiment this improved detection capability has allowed us to observe sharp structures in the kinetic energy distribution and local minima in

the angular distributions along the laser polarization axis, which had escaped observation in earlier experiments.

If the laser polarization is chosen in the plane of the MCP detector, then the 3D velocity distribution has an axis of symmetry in the detection plane. Therefore, the 2D projection contains enough information to reconstruct the 3D velocity distribution by means of an iterative projection procedure which has recently been developed in our group and which is described in more detail elsewhere [23]. Briefly, a trial 3D velocity distribution is assumed, based on the radial and angular distribution observed in the 2D experimental image. From this assumed 3D velocity distribution a 2D projection is calculated, which is compared with the experimentally observed 2D projection. The differences between the calculated and the experimental 2D projections are evaluated and used to apply a correction to the 3D velocity distribution. This procedure is repeated until the differences between the calculated and the experimental 2D projections are acceptably small. Unlike the commonly used Abel inversion procedure (which tends to accumulate noise on the symmetry axis ($v_x = v_y = 0$) where the noise interferes with the accurate determination of angular distributions) our new inversion procedure projects the noise in the experimental image towards the centre of the 3D velocity distribution ($v = 0$), enabling us to obtain much cleaner angular distributions for non-zero kinetic energies.

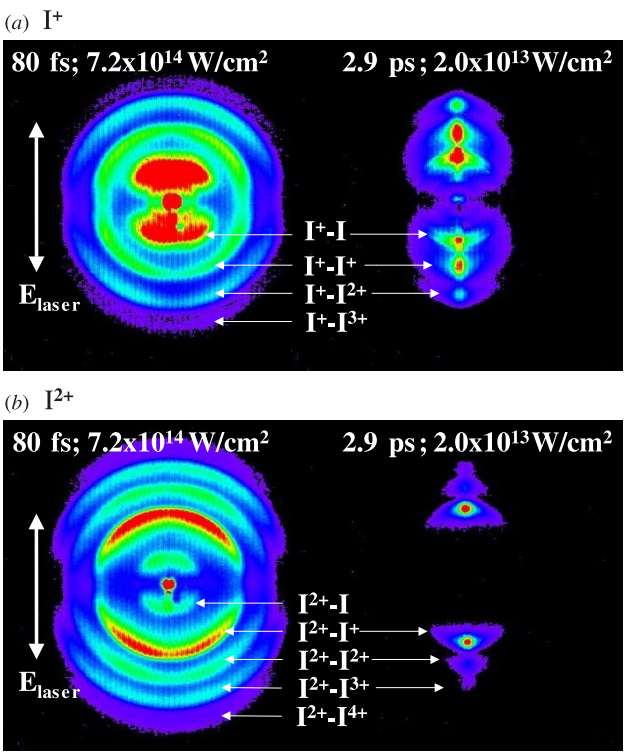

Figure 2. Experimental observation of (*a*) I^+ (*b*) and I^{2+} fragments resulting from the multi-electron dissociative ionization (MEDI) of I_2 for short and long laser pulses. The pulse durations and intensities are indicated in the figure. The laser polarization is along the vertical axis in the plane of the image.

3. Experimental results

In the experiments presented in this paper the influence of the laser pulse duration and pulse energy on the I^{n+} and Br^{m+} fragment angular and kinetic energy distributions resulting from the multi-electron dissociative ionization (MEDI) of I_2 and Br_2 were investigated, using a velocity map imaging detector. Typical experimental images are shown in figure 2 (I_2) and figure 3 (Br_2). The laser polarization axis corresponds to the vertical axis in these pictures. Individual rings correspond to fragment ions with kinetic energies that are characteristic for specific ionization channels. The left-hand sides of figures 2 and 3 give the I^+, I^{2+}, Br^+ and Br^{2+} signals obtained with an 80 fs, 7.2×10^{14} W cm^{-2} pulse for I^+ and I^{2+}, and with an 80 fs, 1.35×10^{15} W cm^{-2} pulse for Br^+ and Br^{2+}. These 80 fs results will from now on be referred to as the short-pulse regime. The right-hand sides of figures 2 and 3 give the I^+, I^{2+}, Br^+ and Br^{2+} signals for a 2.9 ps, 2.0×10^{13} W cm^{-2} pulse for I^+ and I^{2+} and for a 2.5 ps, 4.3×10^{13} W cm^{-2} for Br^+ and Br^{2+}. These results will from now on be referred to as the long pulse regime. In other words, the iodine and the bromine results were obtained with 1 and 2.7 mJ pulses, respectively, which were chirped from their minimum value of 80 fs to pulse durations of 2.9 ps (iodine) and 2.5 ps (bromine). Comparing the images for the short and long pulse regime one can see a substantial narrowing of the angular distribution along the laser polarization axis in the long pulse situation. In the next subsection, this information is quantified by analysing the angular distribution of these images for all the

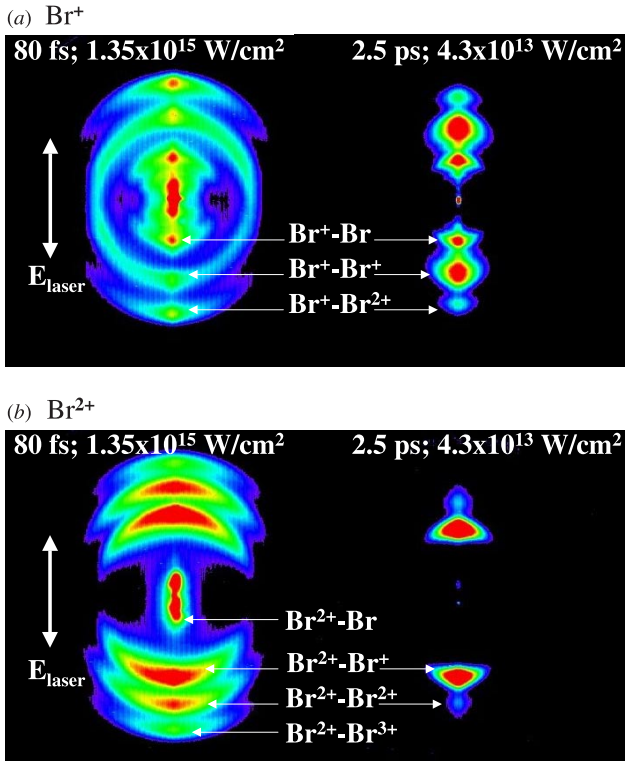

Figure 3. Experimental images of (*a*) Br^+ and (*b*) Br^{2+} fragments resulting from the multi-electron dissociative ionization (MEDI) of Br_2 for short and long laser pulses. The pulse durations and intensities are indicated in the figure. The laser polarization is along the vertical axis.

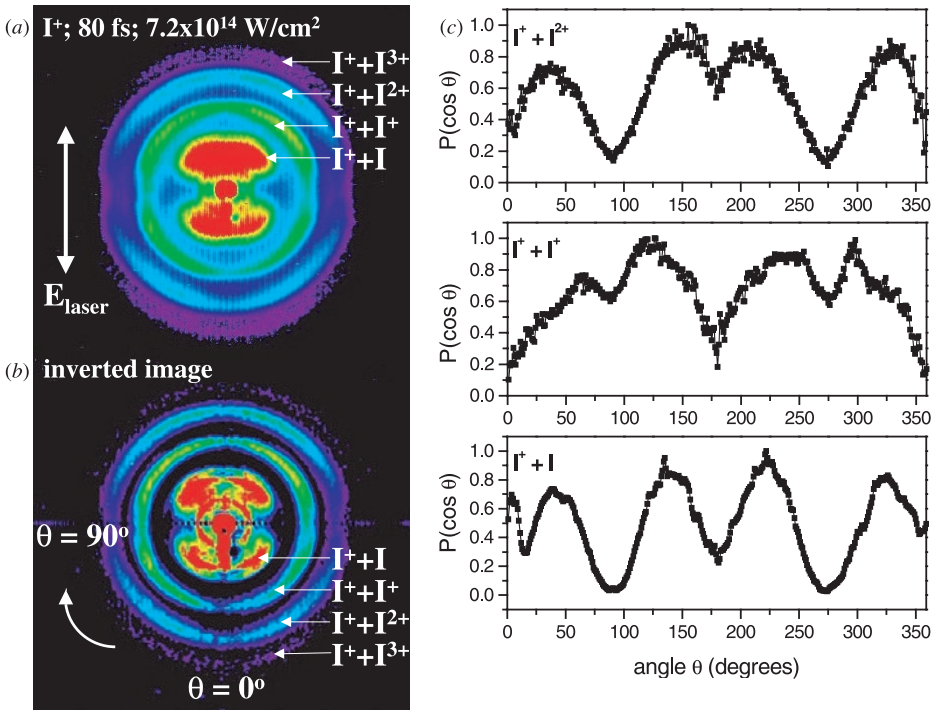

Figure 4. Example of an experimental and an inverted image illustrating the inversion procedure used to extract the 3D velocity distribution from the measured 2D images: (*a*) experimental image presented in figure 2(*a*) for I^+ formed in the Coulomb explosion of I_2 using an 80 fs, 7.2×10^{14} W cm^{-2} pulse; (*b*) slice through the 3D velocity distribution obtained after the inversion procedure presented in section 2; (*c*) angular distribution of the individual ionization channels. For the definition of θ see (*b*).

different charge channels systematically as a function of the laser pulse energy and the laser pulse duration.

3.1. Angular distribution

From the 2D distributions presented in figures 2 and 3, one can extract the angular distributions for I^+, I^{2+}, Br^+ and Br^{2+} fragments resulting from different ionization channels for the long and short-pulse regimes. An example of how the 3D velocity distribution is obtained from the 2D projected image and how the angular distribution is extracted from this 3D distribution is shown in figures 4 and 6 for I^+ fragments created using a short (80 fs) and a long (2.9 ps) pulse, respectively, in both cases with 1 mJ pulse energy (i.e at intensities of 7.2×10^{14} W cm^{-2} and 2.0×10^{13} W cm^{-2}, respectively). In figure 4(*a*) the data presented in figure 2(*a*) are reproduced, where the I^+ signal was obtained with an 80 fs pulse duration. In figure 4(*b*) a cut through the 3D velocity distribution is presented, which was obtained using the inversion procedure explained in section 2. Unlike in the 2D projected image, fragments corresponding to different ionization channels are completely separated in the 3D cut. In the image presented in figure 4(*a*) a slow modulation can be noticed, which is caused by the CCD camera. This modulation was removed by Fourier filtering prior to the inversion procedure. The sharp structure, which appears around the centre of the $I^+ + I$ image in figure 4(*a*) and which is even

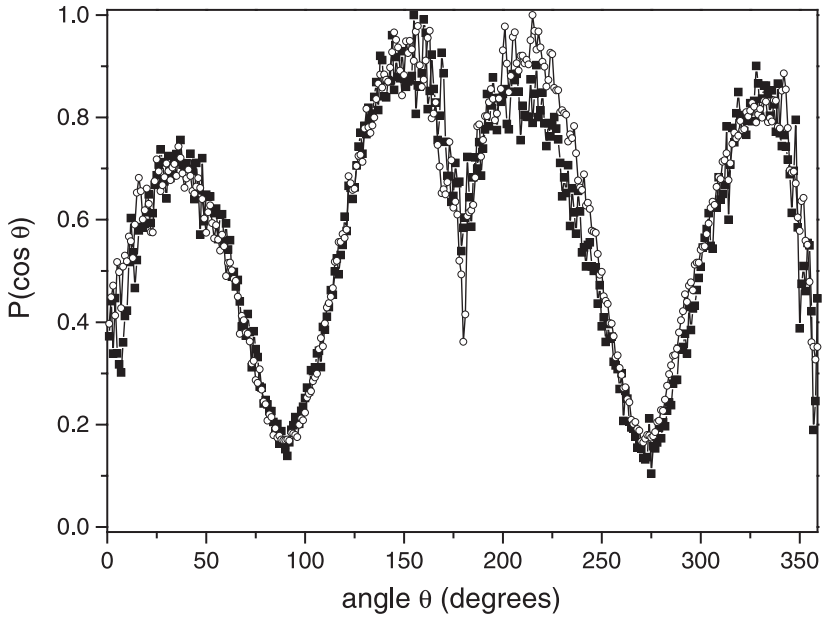

Figure 5. Angular distributions of the I^+ (full squares) and I^{2+} (open circles) fragments resulting from the $I^+ + I^{2+}$ channel formed in the Coulomb explosion of I_2 using an 80 fs, 7.2×10^{14} W cm^{-2} pulse (see figures 1(*a*) and (*b*)).

more visible in the inverted image, will be discussed in the subsection on fragment kinetic energy distributions.

The angular distributions obtained from the 3D velocity distribution are shown in figure 4(*c*). The angular distributions are obtained by integrating contributions in the 3D velocity distribution corresponding to different ionization channels over the relevant velocity range and over the azimuthal angle ϕ. The angular distributions are given as a function of the angle θ between the laser polarization axis (the vertical axis in the images) and the atomic recoil direction, which coincides with the molecular axis. As indicated, $\theta = 0$ corresponds to the bottom of the cut shown in figure 4(*b*), and increases clockwise. Since in spherical coordinates the size of a volume element is equal to $\mathrm{d}v \sin\theta \, \mathrm{d}\phi \, \mathrm{d}\theta$ integration of the 3D velocity distribution $P(v, \theta, \phi)$ over v and ϕ leads to a determination of $P(\cos\theta)$. If the angular distribution is isotropic, then $P(\cos\theta)$ is constant. To be able to compare the angular distributions of different channels they have been normalized individually. The angular distributions typically have minima at 90° and 270° (perpendicular to the laser polarization axis) and maxima at 0° and 180° (along the laser polarization). For very short pulses the distributions have a hole in the centre (at 0° and 180°) which is less deep for higher charge channels (see figure 4(*c*)). We believe that the explanation for this hole, which has not been reported in earlier measurements using time-of-flight techniques [2, 10, 13], is likely to be that molecules that are aligned along the polarization axis can more easily reach higher charge states and therefore fewer ions remain in lower charge states in this direction. Some evidence for this is given by our modelling of the MEDI process [19]. The width of the angular distribution is narrower for higher charge states. This is because the higher charge ionization channels require the absorption of a higher number of photons [13, 19]. The asymmetry between the lower part and the upper part of the images (at 0° and 180°), and the appearance of a dark area near the centre of the image

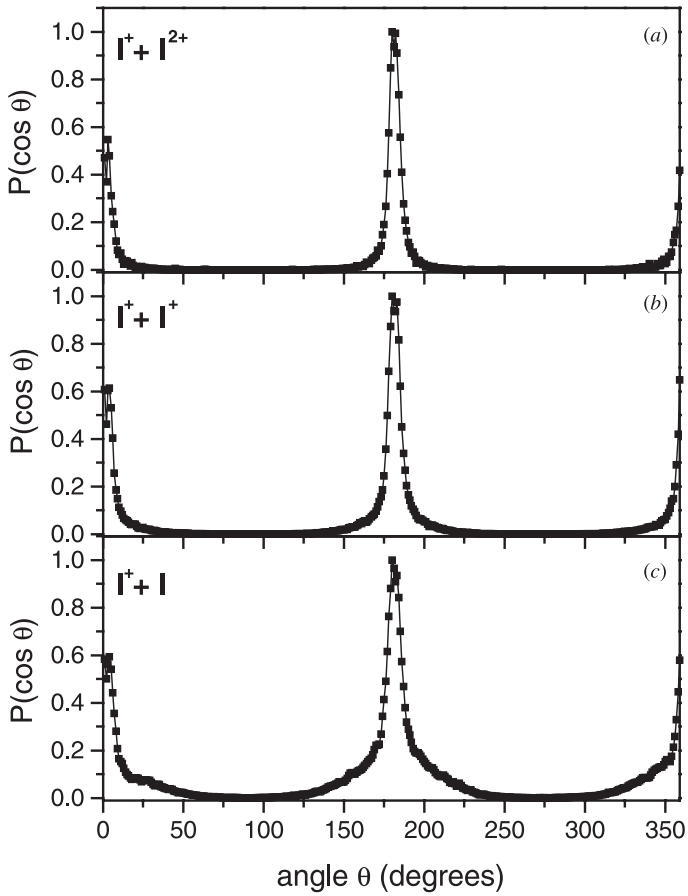

Figure 6. Angular distributions obtained from figure 2(*a*) after the inversion procedure, for I^+ fragments resulting from the Coulomb explosion of I_2 for a 2.9 ps, 2.0×10^{13} W cm^{-2} pulse. Different curves correspond to different ionization channels (as indicated in the figure). We note that the pedestal which appears underneath the narrow peak influences the width of the Gaussian fit used to calculate the FWHM for the angular distributions, which yields a FWHM of (*a*) 11.8°, (*b*) 17.4° and (*c*) 33.7°.

(which leads to some artefacts in the angular distribution of the $I^+ + I$ channel) are due to slight inhomogeneities of the detector as a result of extended use.

For the triply ionized iodine molecule I_2^{3+}, one of the dissociation channels is the formation of $I^+ + I^{2+}$. The I^+ and I^{2+} fragments resulting from this channel can be detected independently and from momentum conservation one expects the angular distributions of the two fragments to be the same. In figure 5 the angular distributions of the I^+ and I^{2+} signal resulting from the $I^+ + I^{2+}$ channel are presented, for the measurements obtained with 80 fs, 7.2×10^{14} W cm^{-2} laser pulses (see figure 2(*a*) and (*b*)). The similarity of the two curves shows the accuracy of the experimental method.

In figure 6 the angular distributions of the I^+ fragments are shown for the data presented in figure 2(*a*), obtained for 2.9 ps, 2.0×10^{13} W cm^{-2} laser pulses. Again the angular distributions have a maximum along the laser polarization axis and a minimum perpendicular to it, and become narrower in higher charge channels. Comparing the width of the angular distributions

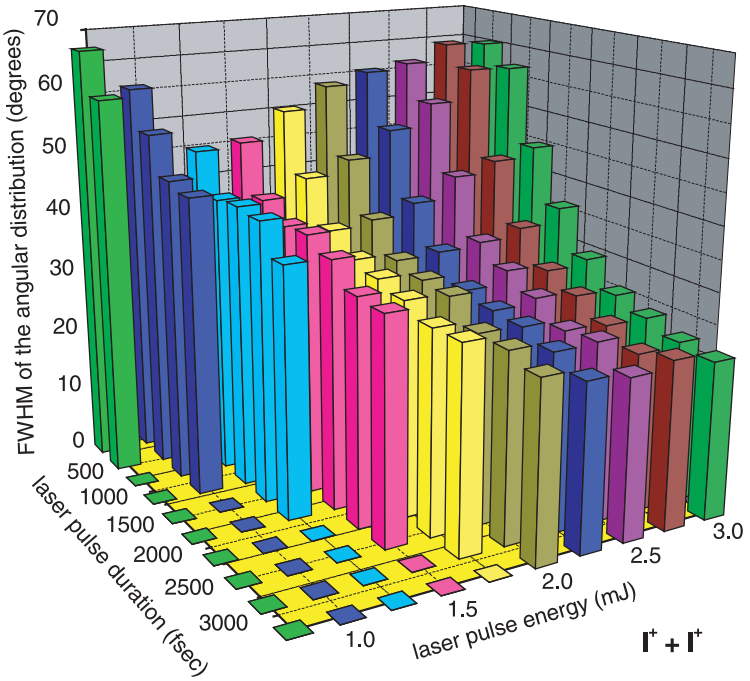

Figure 7. The FWHM of the angular distribution versus the laser pulse duration and laser pulse energy for the I^+ signal resulting from the $I^+ + I^+$ channel formed in the Coulomb explosion of I_2. The FWHM are calculated by a Gaussian fit of the experimental angular distribution after the inversion, as shown in figure 4. The pulse duration is given in fs and the pulse energy is given in mJ. Based on a calibration of the absolute intensity using ATI in Xe, the intensity in the measurement is equal to $(2.65 \times 10^{16})\ E\ (\mathrm{mJ})/\Delta t\ (\mathrm{fs})\ \mathrm{W\ cm^{-2}}$.

in the short-pulse regime (figure 4(*c*)) and in the long pulse regime (figure 6), one clearly sees that the fragment angular distributions are significantly narrower for longer pulses. For low charge states a pedestal is present in the angular distributions. From our simulations of the dissociative ionization process [19] we believe the pedestal to be due to a volume effect. The angular distributions for individual charge states become wider as a function of the peak intensity. Integrating over the focal volume, molecules exposed to a relatively low intensity will contribute only to the low charge channels with a narrow angular distribution, while molecules exposed to a higher intensity contribute with a wider angular distribution to the low charge fragment channels and with a narrow angular distribution to the higher charge channels. Therefore, the angular distribution is given by an average over narrow and wide angular distributions.

The angular distributions for long pulse durations are approximately Gaussian, whereas for very short pulses they are somewhat non-Gaussian, involving four-lobed distributions with a minimum near 0° and 180°. Although a Gaussian fit is a crude approximation to some of the angular distributions, we calculated the FWHM (full width at half maximum) for a Gaussian fit for all angular distributions in order to quantitatively compare the distributions for different pulse durations and pulse energies. Taking into account that the measured 2D images are symmetric with respect to both the laser propagation axis and the laser polarization axis, every quadrant of the experimental image represents a complete and independent measurement of the 3D velocity distribution. The FWHM is therefore calculated as the average of the values

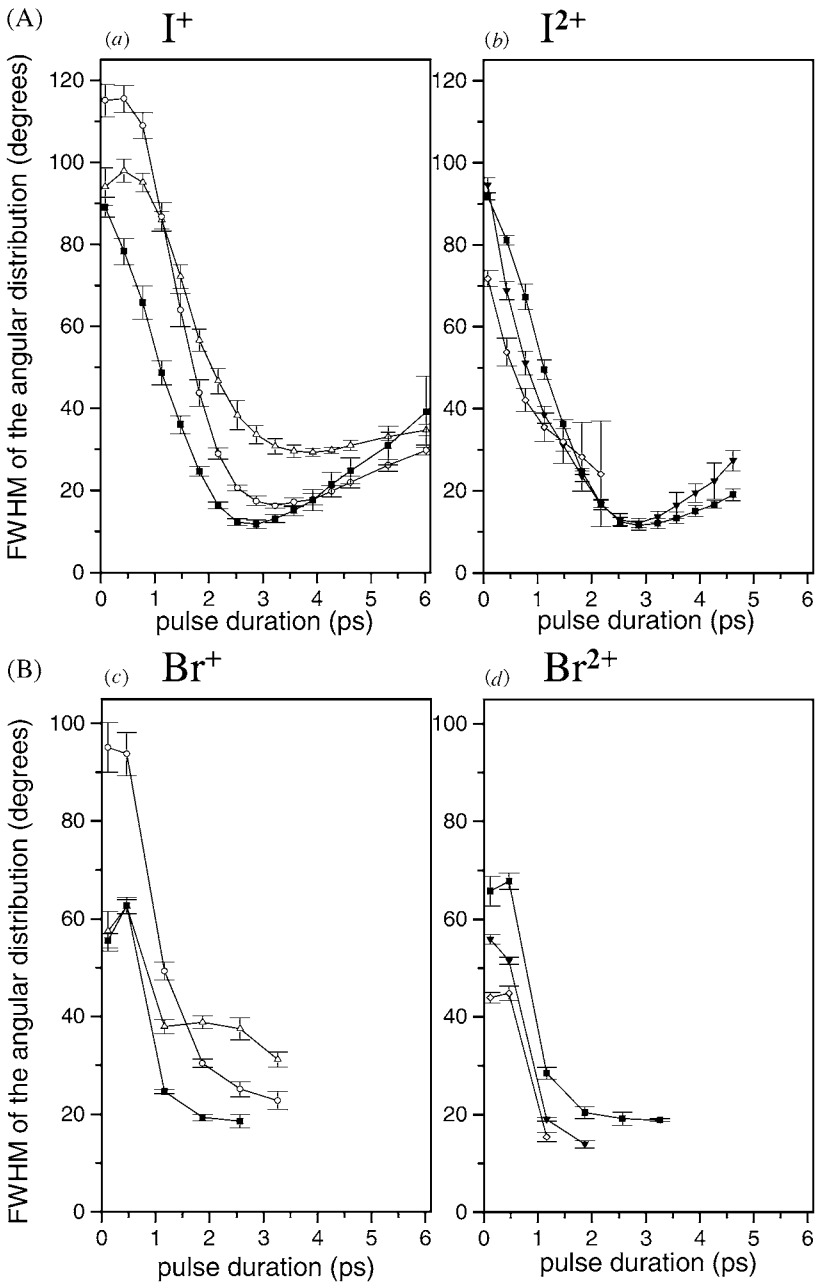

Figure 8. The FWHM of the angular distribution versus laser pulse duration for (A) I_2 and (B) Br_2. The laser fluence was 58 J cm^{-2} for I_2 and 96 J cm^{-2} for Br_2. (*a*) I^+ from $I^+ + I$ channel (open triangles), $I^+ + I^+$ channel (open circles), $I^+ + I^{2+}$ channel (full squares); (*b*) I^{2+} fragments $I^{2+} + I^+$ channel (full squares), $I^{2+} + I^{2+}$ channel (full triangles), $I^{2+} + I^{3+}$ channel (open diamonds); (*c*) Br^+ fragments from $Br^+ + Br$ channel (open triangles), $Br^+ + Br^+$ channel (open circles), $Br^+ + Br^{2+}$ channel (full squares); (*d*) Br^{2+} fragments from $Br^{2+} + Br^+$ channel (full squares), $Br^{2+} + Br^{2+}$ channel (full triangles), $Br^{2+} + Br^{3+}$ channel (open diamonds).

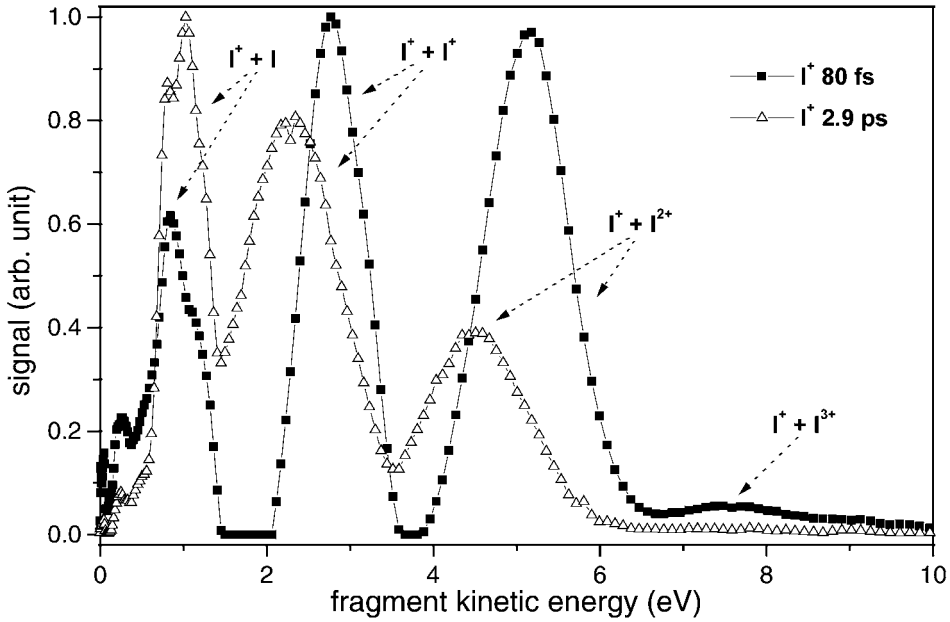

Figure 9. Kinetic energy distribution of the I^+ fragments formed in the Coulomb explosion of I_2 for 80 fs (squares) and 2.9 ps (triangles) laser pulses at a laser fluence of 58 J cm^{-2}. The sharp structure that appears at low kinetic energy is discussed in the text.

obtained from all four quadrants of the images, and error bars are calculated based on the differences encountered in the four quadrants.

In figure 7 the FWHM of the angular distribution of the I^+ fragments resulting from the $I^+ + I^+$ channel, is given as a function of the pulse energy and the pulse duration. In this 3D graph the pulse duration is given in fs and the pulse energy is given in mJ. Based on a calibration of the intensity using ATI in Xe, the intensity in the measurement can be calculated as $I = (2.65 \times 10^{16})\ E\ (\mathrm{mJ})/\Delta t\ (\mathrm{fs})\ \mathrm{W\,cm^{-2}}$. Figure 7 shows that for constant pulse duration, the FWHM of the angular distribution depends only weakly on the laser pulse energy, showing a small decrease with increasing energy, except for very short pulses, where the FWHM increases again for the highest pulse energies. However, if the pulse duration is increased at a constant laser energy, the FWHM of the angular distribution decreases substantially. For example, the FWHM decreases from $64.4 \pm 2.0^\circ$ to $25.2 \pm 0.8^\circ$ when at a pulse energy of 3 mJ the pulse duration is stretched from 500 fs to 3 ps (corresponding to a reduction in the intensity from 1.6×10^{14} W cm^{-2} to 2.65×10^{13} W cm^{-2}). A detailed discussion of the results of figure 7 will be presented in section 4, following a discussion of the extended Coulomb explosion model.

The measurements shown in figure 7 were performed using Ar as seed gas. Here, space charge effects precluded the use of laser pulses with pulse durations < 500 fs. Using Ne as seed gas, the experiments could be extended to shorter pulse durations. This series of measurements further illustrates the role of the pulse duration (see figure 8). In figures 8(*a*) and (*b*) the FWHM of the angular distributions for individual I^+ and I^{2+} channels are presented as a function of the laser pulse duration, at a constant laser fluence of 58 J cm^{-2}. All ionization channels exhibit similar behaviour. The width of the angular distribution is largest for short pulses, narrows and reaches a minimum for a longer pulse duration that depends on the channel (e.g. for $I^+ + I$ at 3.9 ps, for $I^+ + I^+$ at 3.2 ps, for $I^+ + I^{2+}$ at 2.9 ps) and then starts increasing again

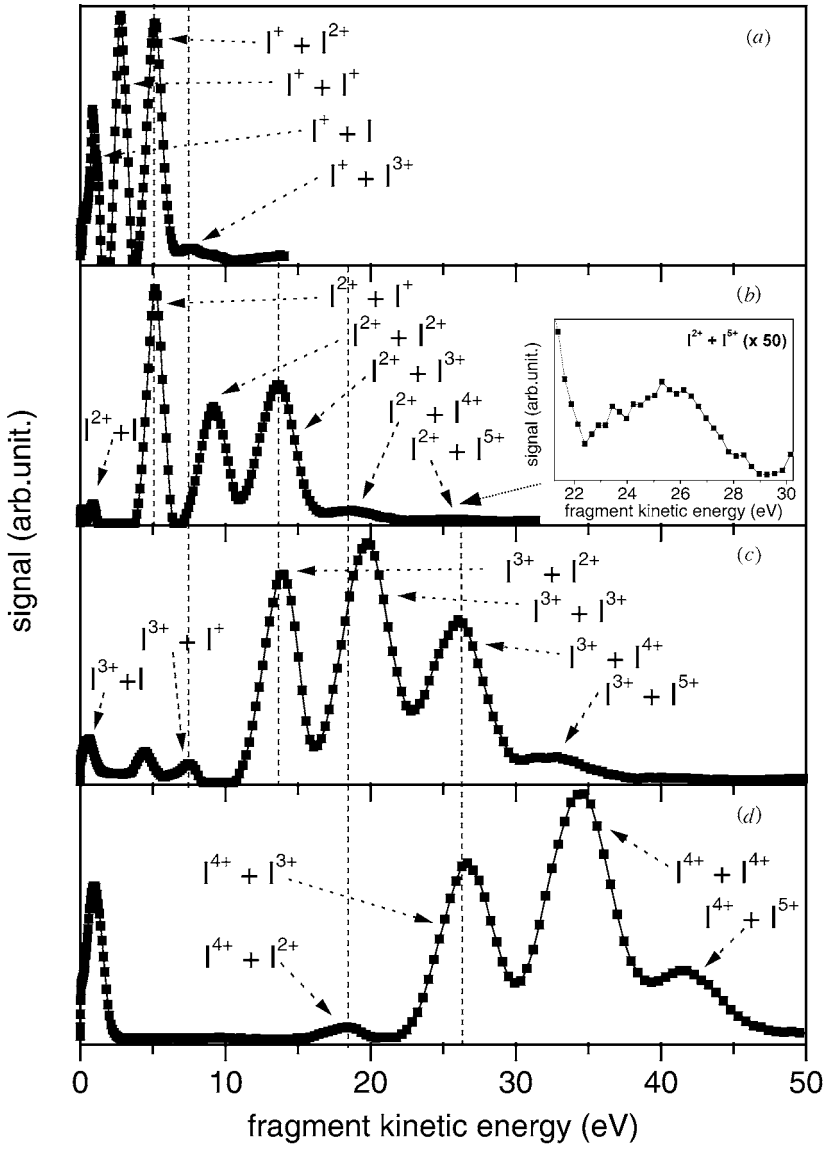

Figure 10. Kinetic energy distribution of different charged fragments resulting from the Coulomb explosion of I_2 for an 80 fs, 7.2×10^{14} W cm^{-2} pulse. The peaks in the kinetic energy distributions of the (*a*) I^+, (*b*) I^{2+}, (*c*) I^{3+} and (*d*) I^{4+} fragments correspond to the ionization channels indicated in the figures. The dotted lines connect fragments resulting from the same channel. The insert in part (*b*) shows a magnification of the $I^{2+} + I^{5+}$ channel.

as the pulse duration is increased further. For the $I^+ + I$ channel the maximum width of the angular distribution does not occur for the shortest pulse duration but for longer pulses (500 fs) (figure 8(*a*)). As before, the behaviour of different fragments resulting from the same channel is similar within the experimental error (e.g. I^+ and I^{2+} resulting from the $I^+ + I^{2+}$ channel).

The narrowing of the FWHM of the angular distributions for longer pulse durations observed for I_2 can similarly be seen in the case of Br_2. In figures 8(*c*) and (*d*) the FWHM of

the angular distributions for individual Br^+ and Br^{2+} channels are presented as a function of the laser pulse duration, at a constant laser fluence of 96 J cm^{-2}. The evolution of the width of the angular distribution for Br_2 fragments is similar to that of I_2 fragments except that the pulse duration for which the FWHM reaches a minimum is smaller (~ 2 ps for all the channels). As we will also see in the theoretical model to be discussed in section 4, a comparison of figures 8(*a*) and (*b*) with figures 8(*c*) and (*d*) shows that Br_2 molecules adapt to the laser field more rapidly than I_2 molecules.

3.2. Fragment kinetic energy distribution

The kinetic energy of the fragments in a Coulomb explosion depends on the charge of the fragments and the internuclear distance at which the fragments reach their final ionization state. Experimentally, the kinetic energy of the fragments can be obtained from the 3D velocity distributions following inversion of the measured images [23]. Figure 9 shows the energy distribution of I^+ fragments obtained using 1 mJ pulses with a 80 fs (7.2×10^{14} W cm^{-2}) and a 2.9 ps (2.0×10^{13} W cm^{-2}) pulse duration, respectively. For the longer pulses the kinetic energy of the fragments is smaller. This will be explained in more detail in section 4.

Figure 10 shows the energy distributions of the I^+, I^{2+}, I^{3+} and I^{4+} fragments obtained using an 80 fs, 7.2×10^{14} W cm^{-2} laser pulse. The kinetic energies of different fragments from the same ionization channels are equal within the experimental errors (the vertical lines in figure 10 connect the fragments of the same ionization channels). It is important to note that channels with high charge asymmetry have been detected (e.g. $I^{2+} + I^{5+}$).

In some of the images we have observed sharp structures for the low charge channels $I^+ + I$ and $Br^+ + Br$ (see, e.g., in figures 2(*a*) and 3(*a*)). These contributions are clearly visible in the fragment kinetic energy distributions presented in figure 9 for iodine fragments (below 1 eV) and similarly for bromine fragments (not shown here). The sharp structures may be due to resonances, that appear in the ionization process and/or photodissociation of I_2/Br_2, followed by ionization of one of the atomic fragments. This is supported by the fact that the sharp structure is especially visible for longer laser pulses. Gordon and co-workers [24] recently reported velocity map imaging of dissociative ionization of I_2 at intermediate intensities (10^{10}–10^{12} W cm^{-2}), using a narrowband tunable laser with a nanosecond pulse duration. They observed peaks in the fragment recoil kinetic energy distribution which were attributed to channels involving production of neutral and singly charged iodine atoms in various spin–orbit states, as well as ion-pair states. It is likely that similar mechanisms are responsible for the sharp structures in our experiments.

4. The extended Coulomb explosion model

When diatomic molecules are subjected to laser intensities $\geqslant 10^{13}$ W cm^{-2}, multi-electron dissociative ionization (MEDI) occurs. Ions are predominantly ejected along the E-field of a linearly polarized laser and have kinetic energies that are typically about half of that expected from a Coulomb explosion at the equilibrium internuclear distance of the molecule. Both of these observations have been explained by the field-ionization Coulomb-explosion model [8]. This model allows the calculation of the minimum laser intensity required for over-the-barrier ionization, as a function of the internuclear distance. Geometric alignment arises in this model as a consequence of the reduction of the Stark shift experienced by the electron when the internuclear axis is at an angle with respect to the laser polarization axis [10]. The characteristic kinetic energies are associated with the enhancement of the ionization probabilities at a critical internuclear separation where the ionization threshold is lowest. Here the central barrier

between the two atoms has risen to such an extent that it strongly inhibits adiabatic adjustment to the laser field, and localization of the outer electron on one of the two atoms occurs. To simulate the results of our experiment we have extended this model (similar to the work in [17]) by including the dynamic rotation of the molecule induced by the laser field [25]. Our model calculations are presented only briefly in this paper and are the subject of a companion paper published separately [19].

The extended Coulomb explosion model makes explicit use of the fact that the ionization takes place in the tunnelling regime. Depending on the ionization potential, the laser intensity and the laser wavelength, ionization takes place in the tunnelling or the multiphoton regime. The transition between these regimes is described by the Keldysh parameter $\gamma = (\mathrm{IP}/2E_{\mathrm{ponderomotive}})^{1/2}$, where IP is the ionization potential and the ponderomotive energy $E_{\mathrm{ponderomotive}} = e^2\varepsilon^2/4m\omega^2$, where ε is the electric field strength of the laser and ω the laser frequency. For $\gamma > 1$ (intensities below approximately 10^{14} W cm^{-2} using 800 nm light) the ionization is a multiphoton process, whereas for $\gamma < 1$ it is a tunnelling process. In our experiment the initial ionization takes place at intensities near 10^{13} W cm^{-2} and is a multiphoton process, whereas the subsequent Coulomb explosion steps are progressively better described as tunnelling processes. Indeed, this is the way they are modelled in the extended Coulomb explosion model.

In MEDI the laser field not only ionizes and dissociates the molecule, but also induces a torque that depends on the anisotropic polarizability of the molecules, and causes a damped oscillation of the molecule around the polarization axis of the laser until ionization and dissociation takes place. This process depends on three factors: (a) the peak intensity, (b) the temporal duration of the laser pulse, and (c) the ratio between the anisotropic polarizability and the moment of inertia (α/I). The angular motion of the molecules in the laser field is given by [11, 17]:

$$\frac{\mathrm{d}^2\theta}{\mathrm{d}t^2} = \frac{-\alpha_{\mathrm{eff}}}{4I(t)}\varepsilon(t)^2 \sin 2\theta - 2\frac{1}{R(t)}\frac{\mathrm{d}R(t)}{\mathrm{d}t}\frac{\mathrm{d}\theta}{\mathrm{d}t}$$

where θ is the angle between the laser polarization axis and the internuclear axis, α_{eff} is the anisotropic polarizability ($\alpha_{\mathrm{eff}} = \alpha_{\parallel} - \alpha_{\perp}$), $I(t)$ is the time-dependent moment of inertia $\mu R(t)^2$, $\varepsilon(t)$ is the envelope of the electric field of the laser and $R(t)$ is the internuclear separation. The second term is a damping term that leads to a reduced acceleration as the molecule dissociates (due to conservation of the angular momentum). Note that apart from the parameters appearing in the equation for the angular motion, the mass of the molecule (included in the momentum of inertia) affects the speed at which the Coulomb explosion takes place and the ionization threshold affects how much the molecule rotates before it falls apart.

4.1. Comparison between experiment and theory

We have used this model to calculate the dependence of the fragment ion alignment from the Coulomb explosion as a function of the pulse duration and the pulse energy. Results of the model calculations are shown in figure 11, which shows a comparison between the experimental (see figure 8) and theoretical FWHM in various fragment ion channels, as a function of the laser pulse duration (at fixed laser fluences of 58 J cm^{-2} in the case of I_2 and 96 J cm^{-1} in the case of Br_2). The model predicts that the molecules become strongly aligned for pulses of a few picoseconds, although there is some alignment even at 500 fs. For a given pulse duration, the moment in time where the molecules ionize and subsequently dissociate, limits the amount of alignment that can be reached. Considering also that at a fixed pulse energy the peak intensity is inversely proportional to the pulse duration, this means that the alignment

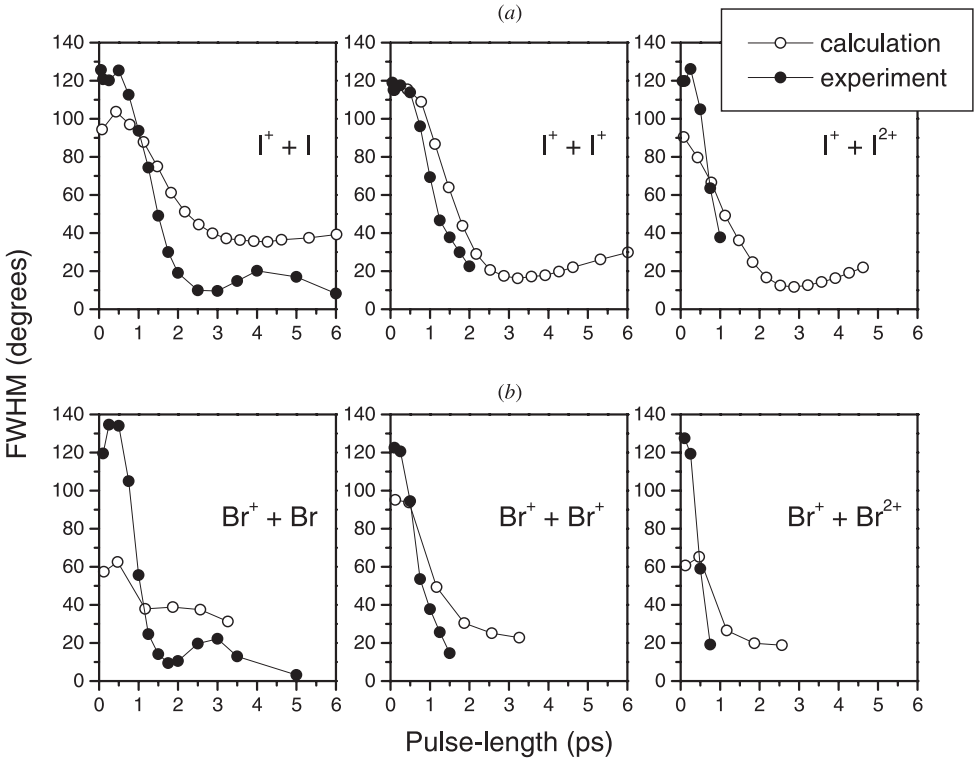

Figure 11. Comparison between the FWHM of the angular distributions as a function of the laser pulse duration obtained experimentally (open circles) and calculated theoretically (full circles) using the model outlined in the text, for laser fluences of 58 J cm^{-2} (I_2) and 96 J cm^{-2} (Br_2). The different graphs represent individual ionization channels (as indicated in the figure) resulting from the Coulomb explosion of (*a*) I_2 and (*b*) Br_2 molecules.

increases with increasing pulse duration. In the case of I_2, the width of the experimental and modelled angular distributions reaches a minimum value for a pulse duration around 3 ps. This minimum in the width of the angular distribution is a manifestation of the fact that the molecules undergo a damped oscillation around the laser polarization axis. For a 3 ps pulse duration a large fraction of the molecules cross the laser polarization axis around the time that the laser intensity reaches the threshold intensity for ionization. For pulses longer than this optimum value, we anticipate that the angular distribution has a further damped oscillatory structure, and the alignment dynamics approaches the adiabatic regime that was studied by Stapelfeldt and co-workers [7]. By averaging over all the I^+ ions from the $I^+ + I$ channel for I_2 seeded in argon Larsen *et al* found that $\langle\langle\cos^2\theta\rangle\rangle = 0.8$ for a 3.5 ns second harmonic YAG laser pulse with a peak intensity of 1.4×10^{12} W cm^{-2}. This corresponds to a value for the FWHM of the angular distribution of 26.6°. We cannot directly compare our results with the results obtained by Larsen *et al* because the FWHM of the angular distribution depends, as could be seen above, not only on the pulse duration but also on the intensity and the wavelength of the laser and the seed gas (which influences the initial rotational temperature of the studied molecules).

The equation for the angular motion shows that the laser-induced angular acceleration depends on the ratio of the anisotropic polarizability to the moment of inertia of the molecule.

I_2 has a higher polarizability than Br_2 ($\alpha_{\text{iodine}} = 45$, $\alpha_{\text{bromine}} = 28$ au), but the momentum of inertia of I_2 ($\mu = 63.5$, $r_{\text{equilibrium}} = 5.04$ au) is substantially larger than the moment of inertia of Br_2 ($\mu = 40.0$, $r_{\text{equilibrium}} = 4.31$ au) so the I_2 molecules adapts more slowly to the laser field, as observed experimentally. Furthermore, the ionization potential of Br_2 is higher than the ionization potential of I_2 ($\text{IP}_{\text{iodine}} = 9.3$, $\text{IP}_{\text{bromine}} = 10.45$ eV), which means that under identical laser conditions the ground state Br_2 molecules experience the alignment force for a longer time than their I_2 counterparts, leading to narrower angular distributions in the case of Br_2. The differences between MEDI of I_2 and Br_2 are further elaborated in our companion paper describing the model calculations performed [19].

4.2. Discussion

As shown in figure 7 the FWHM of the angular distribution initially decreases when the intensity is increased by increasing the pulse energy at a constant pulse duration, but then increases when the intensity is increased further, either by increasing the pulse energy at constant pulse duration (see results for $\leqslant 1.5$ ps pulse duration) or by decreasing the pulse duration (see results at all pulse energies). At the lowest energies where experiments were performed, broad angular distributions are observed due to geometric alignment. Upon increasing the laser pulse energy, the FWHM of the angular distribution decreases due to dynamic alignment. If geometric alignment would be the only factor determining the angular distributions then a widening of the angular distributions with increasing laser intensity would be anticipated [10]. In contrast, at all pulse durations, a moderate decrease in the width of the angular distributions with increasing laser pulse energy is experimentally observed, due to an increase in the alignment forces with laser intensity. The increase in the FWHM of the angular distribution when the intensity of the laser pulse is increased further (observed for pulse durations $\leqslant 1.5$ ps) is due to the fact that for laser intensities above the saturation intensity the molecules ionize earlier and earlier on the rising edge of the laser pulse, reducing the amount of dynamic alignment [13,17]. In this short-pulse, high-intensity regime the angular distribution is dominated by geometric effects [10].

In experiments where the peak intensity is constant, we observe a strong decrease in the FWHM of the angular distribution with increasing pulse duration and energy. For example, in the experiments with 1 mJ, 1 ps pulses and with 3 mJ, 3 ps pulses (in both cases reaching a peak intensity of 2.65×10^{13} W cm^{-2}) the FWHM of the angular distribution in the $I^+ + I^+$ channel was $54.3 \pm 0.9^\circ$ and $25.2 \pm 0.8^\circ$, respectively. As in the previous discussion of measurements beyond the saturation intensity, the decrease is due to the fact that for a fixed peak intensity the molecules undergo a more extensive dynamic alignment before ionization takes place if the pulse duration is longer. If there were no dynamic alignment, then a widening of the angular distribution with pulse duration (at constant peak intensity) would be anticipated, due to the fact that for longer pulses the molecules can more efficiently reach the critical distance for Coulomb explosion, and hence Coulomb explosion from less-favourable alignment angles becomes possible. The fact that this is not observed experimentally is strong evidence for the presence of dynamic alignment.

The model also reproduces the experimentally observed shift in the kinetic energy release for long laser pulses (see figure 9). This shift has also been observed in previous experiments [8]. For longer pulses, the intensity requirements for ionization are satisfied at later times and longer internuclear distances, where the Coulomb repulsion between the two ionic cores is weaker and the kinetic energy release smaller. In agreement with the work of Posthumus *et al* [8] we observed a significant decrease in the fragment kinetic energy release for long pulses, suggesting that the Coulomb explosion takes place at a larger internuclear distance for

longer pulses (e.g. for 3.9 ps pulses we observe that the kinetic energy release decreases to 80% compared with the release from Coulomb repulsion at the equilibrium internuclear distance of the neutral molecule).

Based on the same argument, the peak width of the different ionization channels in the energy distribution can be explained. The width is caused by the variation of the intensity within the interaction volume. Molecules that experience a lower peak intensity dissociate at a larger internuclear distance into fragments with a smaller kinetic energy release and this results in a spread of the kinetic energies, which is larger for the higher charge channels.

5. Conclusions

In recent years there has been considerable interest in the angular distributions of fragment ions resulting from multi-electron dissociative ionization (MEDI). A central issue has been the question whether observed fragment ion angular distributions are the result of the angular dependence of the ionization process (geometric alignment) or laser-induced reorientation of molecules prior to and during the MEDI process (dynamic alignment). In this paper we have presented results on dynamic and geometric alignment of I_2 and Br_2 molecules, where we have studied fragment ion angular distributions as a function of the laser pulse energy and pulse duration. For heavy molecules, such as I_2 and Br_2, geometric alignment dominates for subpicosecond pulses, where the laser pulse is too short for the molecule to rotate significantly, whereas dynamic alignment becomes important for pulse durations $\geqslant 1$ ps, with an optimum for pulse durations of ~ 2–3 ps. The pulse duration for which the dynamic alignment starts to manifest itself depends on the characteristics of the studied molecule (momentum of inertia, polarizability, mass, ionization potential). The angular distributions are observed to be only weakly dependent on the peak intensity in the experiment. At low intensities an increase in the alignment is observed with increasing intensity, however, this trend reverses for peak intensities exceeding the saturation intensity, when the ionization process takes place earlier in the laser pulse, reducing the role of the dynamic alignment.

The experiments that we have presented in this paper follow the work of several other researchers who have considered the possibility of geometric and dynamic alignment in I_2. Posthumus *et al* studied MEDI of I_2 with 50 fs pulses [10] and concluded on the basis of the intensity dependence of the angular distributions that dynamic alignment did not play a significant role in their experiments. Schmidt *et al* reported measurements of iodine angular distributions for pulse durations of 130 fs and concluded that angular distributions in the low ($q \leqslant 3$) charge channels were determined by geometric alignment, whereas higher ($q > 3$) charge channels were strongly influenced by dynamic alignment [13]. In agreement with this, we find in our experiments that for 80 fs pulses the angular distributions can be understood from geometric alignment, whereas for pulse durations of 500 fs and above dynamic alignment begins to play a significant role.

Our results clearly show the strength of using the velocity map imaging technique. Using velocity map imaging high quality measurements of the angular distribution can be performed very rapidly. For example, all the datapoints in figure 7 were collected within a single day. This is probably the reason why we have been able to see two new features in MEDI of I_2, namely the observation of a minimum in the angular distribution near $\theta = 0^\circ$ for short pulses and the observation of sharp features in the fragment kinetic energy distribution for long pulses, which were not reported before.

The observation of dynamic alignment in MEDI using short ($\sim$1 ps) laser pulses suggests important opportunities for studies with aligned molecules. Under these experimental conditions the time evolution of the molecular rotational wavefunction is strongly non-adiabatic

and the formation of an aligned molecule at the time of ionization in a MEDI process, as inferred from the experiments, suggests the formation of a rotational wavepacket at the end of the laser pulse [26–28] allowing for the preparation of samples of aligned molecules on subsequent revivals of the wavepacket. Indeed, building on the understanding gained from the experiments reported in this paper, we have recently carried out a two-pulse pump–probe experiment in which we have been able to monitor the time-evolution of this rotational wavepacket, including the occurrence of revivals where the angular distribution of the molecule is suddenly narrowed or broadened during a short time interval [29]. Thus far experimental studies with aligned or oriented molecules have been conducted using brute force orientation in strong external electric fields [30] and strong optical fields [7]. Exploiting the generation of a rotational wavepacket in short-pulse excitation of molecules enables the formation of aligned or oriented samples of molecules under field-free conditions, making possible, among other things, studies of molecular frame photoelectron angular distributions.

Acknowledgments

This work is part of the research programme of the 'Stichting voor Fundamenteel Onderzoek der Materie (FOM)', which is financially supported by the 'Netherlandse organizatie voor Wetenschappelijk Onderzoek (NWO)'. ES and CN were supported by Marie Curie Individual Fellowships from the European Community Fifth Framework Training and Mobility of Researchers programme. We would like to acknowledge the technical support of Anton Buijserd, Rob Kemper and Hinco Shoenmaker and thank Arjan Houtepen for helpful discussions.

References

[1] Frasinski L J, Codling K and Hatherly P 1987 *Phys. Rev. Lett.* **58** 2424
[2] Strickland D T, Beaudoin Y, Dietrich P and Corkum P B 1992 *Phys. Rev. Lett.* **68** 2755
[3] Friedrich B and Herschbach D 1995 *Phys. Rev. Lett.* **74** 4623
[4] Seideman T 1997 *J. Chem. Phys.* **103** 7887
[5] Ortigoso J, Rodriguez M, Gupta M and Friedrich B 1999 *J. Chem. Phys.* **110** 3870
[6] Sakai H, Safvan C P, Larsen J J, Hilligsoe K M, Hald K and Stapelfeldt H 1999 *J. Chem. Phys.* **110** 10 235
[7] Larsen J J, Sakai H, Safvan C P, Wendt-Larsen I and Stapelfeldt H 1999 *J. Chem. Phys.* **111** 7774
[8] Posthumus J H, Giles A J, Thompson M R, Shaikh W, Langley A J, Frasinski L J and Codling K 1996 *J. Phys. B: At. Mol. Opt. Phys.* **29** L525
Posthumus J H, Giles A J, Thompson M R and Codling K 1996 *J. Phys. B: At. Mol. Opt. Phys.* **29** 5811
[9] Seideman T, Ivanov M Yu and Corkum P B 1995 *Phys. Rev. Lett.* **75** 2819
Ivanov M, Seideman T, Corkum P B, Ilkov F and Dietrich P 1996 *Phys. Rev.* A **54** 1541
[10] Posthumus J H, Plumridge J, Thomas M K, Codling K, Frasinski L J, Langley A J and Taday P F 1998 *J. Phys. B: At. Mol. Opt. Phys.* **31** L553
[11] Ellert Ch and Corkum P B 1999 *Phys. Rev.* A **59** R3170
[12] Banerjee S, Ravindra Kumar G and Mathur D 1999 *Phys. Rev.* A **60** R3369
[13] Schmidt M, Dobosz S, Meynadier P, D'Oliviera P, Normand D, Charron E and Suzor-Weiner A 1999 *Phys. Rev.* A **60** 4706
[14] Frasinski L J, Plumridge J, Posthumus J H, Codling K, Taday P F, Divall E J and Langley A J 2001 *Phys. Rev. Lett.* **86** 2541
[15] Normand D, Lompré L A and Cornaggia C 1992 *J. Phys. B: At. Mol. Opt. Phys.* **25** L497
[16] Dietrich P, Strickland D T, Laberge M and Corkum P B 1993 *Phys. Rev.* A **47** 2305
[17] Banerjee S, Mathur D and Ravindra Kumar G 2001 *Phys. Rev.* A **63** 045401
[18] Eppink A T J and Parker D H 1997 *Rev. Sci. Instrum.* **68** 3477
[19] Springate E, Rosca-Pruna F, Offerhaus H L, Krishnamurthy M and Vrakking M J J 2001 *J. Phys. B: At. Mol. Opt. Phys.* **34** 4939
[20] Schyja V, Lang T and Helm H 1998 *Phys. Rev.* A **57** 3692

[21] Proch D and Trickl T 1989 *Rev. Sci. Instrum.* **60** 713
[22] Nicole C, Sluimer I, Rosca-Pruna F, Warntjes J B M, Vrakking M J J, Bordas C, Texier F and Robicheaux F 2000 *Phys. Rev. Lett.* **85** 4024
[23] Vrakking M J J 2001 *Rev. Sci. Instrum.* **72** 4084
[24] Unny S, Du Y, Zhu L, Gordon R J, Sugita A, Kawasaki M, Matsumi Y and Seideman T 2001 *Phys. Rev. Lett.* **86** 2245
[25] Dion C M, Keller A, Atabek O and Bandrauk A D 1999 *Phys. Rev.* A **59** 1382
[26] Charron E, Giusti-Suzor A and Mies F H 1994 *Phys. Rev.* A **49** R641
[27] Seideman T 1999 *Phys. Rev. Lett.* **83** 4971
[28] Long C, Marango J and Friedrich B 2001 *Phys. Rev. Lett.* **86** 775
[29] Rosca-Pruna F and Vrakking M J J 2001 *Phys. Rev. Lett.* **87** 153902
[30] Loesch H J and Remscheid A 1990 *J. Chem. Phys.* **93** 4779